ISBN: 978-3-95450-241-7 ISSN: 2673-5350 doi:10.18429/JACoW-IBIC2022-MOP01

SLS 2.0 – STATUS OF THE DIAGNOSTICS

C. Ozkan Loch†, A. Bonnin, J. Vila-Comamala, N. Samadi, A. M. M. Stampfli, R. Ischebeck
Paul Scherrer Institut (PSI), Villigen PSI, Switzerland

Abstract

In this contribution we give an overview of the diagnostics development for SLS 2.0, focusing on the beam size monitors in the storage ring, the screen monitors for the booster-to-ring transfer line, and beam loss monitors for the storage ring. Test results carried out at the SLS will also be presented. Diagnostics that will only receive a DAQ system upgrade will not be discussed here.

INTRODUCTION

The Swiss Light Source (SLS) synchrotron storage ring will be upgraded to a new diffraction-limited lattice [1], and its booster-to-ring transfer line (BRTL) will also be improved accordingly [2]. The current monitor for the storage ring and charge monitor in the BRTL will be re-used with new DAQ systems but same functionalities [2]. Hence, these systems will not be discussed here.

Up until recently, in the SLS there were beam loss monitors only at the exit of insertion devices. The distributed loss monitor system based on a CMOS camera readout [3] was developed for locating losses around the storage ring. The first prototype monitor was used to locate losses due to a beam dump, to survey possible losses in the first three arcs, and look for changes with respect to undulator gap changes. As a result, the loss detection scintillators were improved. An update on the status of these loss monitors will be discussed later in this proceeding.

Beam size monitoring at the SLS depends on the π-polarization [4] technique, using the visible light at 364 nm from a bend magnet. However, this technique only provides the vertical source size. In order to measure both dimensions of the small source size at SLS 2.0 (< 8 μm), X ray imaging optics based on zone plates will be used. This monitor is based on [5, 6]. The source size will also be monitored in two locations in order to determine the energy spread of the storage ring.

The present screen monitors in the BRTL use a 200 μm Ce:YAG scintillator at 45° angle to visualize the beam. The optical resolution is 30 μm. One of the screen monitors was modified to house a 100 μm Ce:YAG scintillator normal to the beam with a mirror at 45° angle to couple out the scintillation light. The imaging camera and objective were changed and a spatial resolution of 19 μm was achieved. This will be further improved for the new BRTL. The requirements and details are discussed in the next section.

SCREEN MONITORS

The booster-to-ring transfer line (BRTL) will provide nominal injection into the SLS 2.0 storage ring. It also allows performing beam parameter measurements during set up and commissioning. The purpose of the BRTL screen monitors is to determine the beam profiles, transverse emittance and energy spread. The BRTL optics design and layout with the location of all diagnostics components can be found in the SLS 2.0 technical design report [2].

Apart from beam profile measurements in the nominal BTR injection mode, the first BRTL screen will be used for emittance measurements by scanning the upstream quadrupoles, and the second screen will be used for determination of the energy spread. The last screen will be used for the adjustment of the transverse beam size (matching) at the "thick" storage ring injection septum.

Table 1: Screen Monitor Requirements Based on Expected Smallest Beam Size, Required Resolution and Field of View

	Emittance	Energy spread	Thick septum
Beam size	<20 μm	700 μm	<20 μm
Screen resolution	<10 μm	10 μm for precision of 3%	10 μm
FOV dia.	20 mm	20 mm	20 mm

A scintillator crystal (Ce:YAG) will be inserted in the electron beam path by means of linear UHV-feedthroughs and pneumatic controls. To view the entire range of beam motion, the scintillator screen will be normal to the beam with a mirror at 45° angle behind it to couple out the scintillation light (Fig. 1a).

An OTR screen will also be installed at 45° angle with respect to the beam and the camera will be mounted in the Scheimpflug [7, 8] geometry to correct the focal plane. To measure the emittance an iris and focus control of the camera objective is necessary. In order to facilitate simple switching between Ce:YAG and OTR measurements, an optical setup per screen will be installed at the emittance measuring screen monitor (Fig. 1b).

DISTRIBUTED BEAM LOSS MONITOR

It was initially planned to use beam loss detectors based on organic fiber scintillators in the storage ring and BRTL to locate losses and monitor the loss pattern during injection (storage ring filling and top-up operation). Similar to the SwissFEL [9], 2-meter long fiber scintillators were coupled to plastic optical fibers (POF) that guide the scintillator light to the detection system. A CMOS camera was used to image the light from 28 fibers simultaneously.

A system was built and tested at SLS. Injection losses were detected during top-up. The location of the fiber scintillator that gives the highest signals during beam dump supports the radiation measurement results concerning the

† cigdem.ozkan@psi.ch

ISBN: 978-3-95450-241-7 ISSN: 2673-5350 doi:10.18429/JACoW-IBIC2022-MOP01

radiation hotspot. Details of the system and the test results can be found in [3].

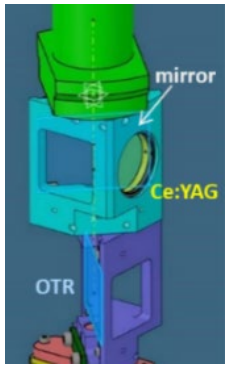

(a)

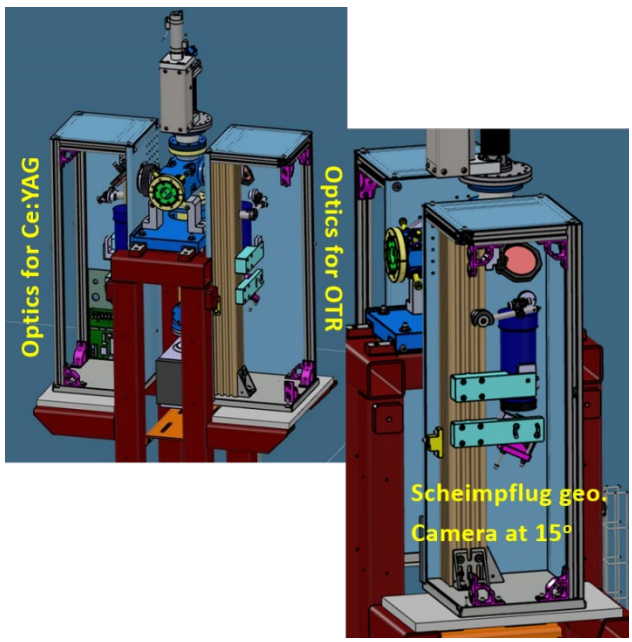

(b)

Figure 1: (a) 3D drawing of the screen holder. The top holder is for the scintillator and mirror, and the second holder is for the OTR screen. (b) Two optical setups are used for the emittance measurement screen: one for imaging the scintillator and the second for the OTR screen. The second is in the Scheimpflug condition.

To test the system sensitivity, we also placed a fiber scintillator at the exit of an undulator and scanned the gap. Although the behaviour matched to an existing loss monitor at the location, the signal difference from one gap setting to the next was too small compared to the existing loss monitor (Fig. 2).

For this reason, a new type of scintillator was used. A plate of EJ-204 [10] was used as the scintillator and the emitted blue light was shifted to green using a wavelength shifting fiber, BCF-92 [11]. An image of this plate scintillator assembly can be found in Fig. 3

For comparison purposes, both scintillators were placed at the same location, at the end of the injection straight. The current of the injection septum was varied to create losses. One POF per scintillator was used to guide the scintillation light from the tunnel to the CMOS camera outside. To account for the difference between the POF fibers, their transmission was measured using an LED and the CMOS camera, and normalized to each other. The behaviour of the two scintillators with varying losses are plotted in Fig. 4. Brightness is the sum of the pixel values in the fiber areas as seen by the camera.

Figure 2: Loss versus Undulator gap setting. Orange is the fiber scintillator readout with the CMOS camera, red is the existing loss monitor, green is the gap reading and blue is the lifetime.

Figure 3: Plate scintillator assembley based on the EJ-204 scintillator and the BCF-92 wavelength shifting fiber, wrapped in foil.

For comparison purposes, both scintillators were placed at the same location, at the end of the injection straight. The current of the injection septum was varied to create losses. One POF per scintillator was used to guide the scintillation light from the tunnel to the CMOS camera outside. To account for the difference between the POF fibers, their transmission was measured using an LED and the CMOS camera, and normalized to each other. The behaviour of the two scintillators with varying losses are plotted in Fig. 4. Brightness is the sum of the pixel values in the fiber areas as seen by the camera.

The new scintillator output is four to five times larger than that of the fiber scintillator. After this measurement, only the new plate scintillators were installed at SLS.

BEAM SIZE MONITOR

Similar to the SLS, the storage ring emittances will be derived from measured source sizes using synchrotron radiation from a bend magnet. However, at SLS 2.0, extrac-

ISBN: 978-3-95450-241-7 ISSN: 2673-5350 doi:10.18429/JACoW-IBIC2022-MOP01

tion of visible light is restricted by the mechanical constraints from the neighbouring magnets. Light coupled out from a narrow opening angle requires the use of X-rays.

A vertical emittance of 10 pm and a horizontal emittance of 158 pm are expected for 6.3% emittance coupling. The optimal, dispersion-dominated, source size is 8.6 µm x 6.8 µm.

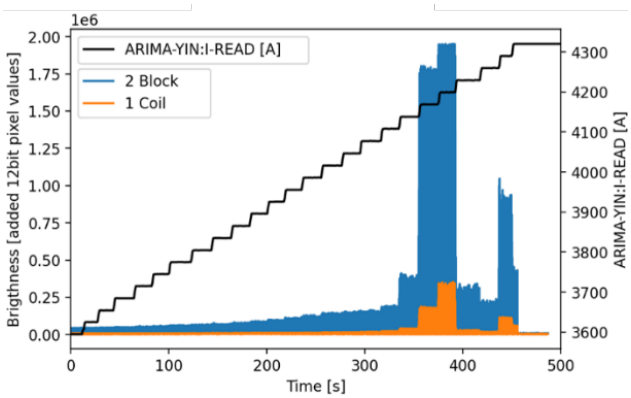

Figure 4: Comparison between the fiber and new scintillators. Orange indicates the behavior of the plastic scintillating fiber, blue indicates the behavior of the plate scintillator, with changing injector magnet current.

tion of visible light is restricted by the mechanical constraints from the neighbouring magnets. Light coupled out from a narrow opening angle requires the use of X-rays.

A vertical emittance of 10 pm and a horizontal emittance of 158 pm are expected for 6.3% emittance coupling. The optimal, dispersion-dominated, source size is 8.6 µm × 6.8 µm.

During machine commissioning, with specified misalignments, a coupling of only 1-2% is expected, which translates to emittance 2-3 pm. With nominal horizontal emittance at full current and open IDs, the vertical emittance will be adjusted to 10 pm to provide sufficient beam lifetime. The range of interest of the vertical emittance to be measured during nominal operation is 8-12 pm. Based on these numbers and the resolution needed to measure an emittance change of 1 pm vertically corresponds to a beam size change of ~400 nm. X-ray optics imaging setup based on Fresnel Zone Plates (FZP) will be used. FZPs allow imaging the beam in 2D and thus, provide size and tilt information simultaneously.

FZPs in transmission geometry are preferred due to their diffraction efficiency reducing photon beam flux and lateral space limitations inside the storage ring tunnel. The first possibility is to use a single zone plate to image the source in the dipole.

We also explore the possibility of using a transmission X-ray microscope (TXM) using two FZPs to shape the image using a condenser zone plate (CZP) [12] and a magnifying zone plate (MZP). This would relax the resolution requirements on the detector. A sketch of the two setups is shown in Fig. 5.

The source size was measured at the TOMCAT beamline at the SLS, with monochromator set to 11.5 keV. The focus of the single zone plate setup was found by varying detector to CZP distance. A plot of the source size with respect to detector location is given in Fig. 6. For the detector, a 5 µm thick LSO:Tb scintillator with 20x microscope objective and a pco.edge camera (pixel size: 6.5 µm) was used. The primary beam was suppressed by placing a central stop (CS) in front of the CZP. The minimum vertical source size was measured as 18.3 µm (rms) and at that detector location the horizontal source size is 78.7 µm (rms).

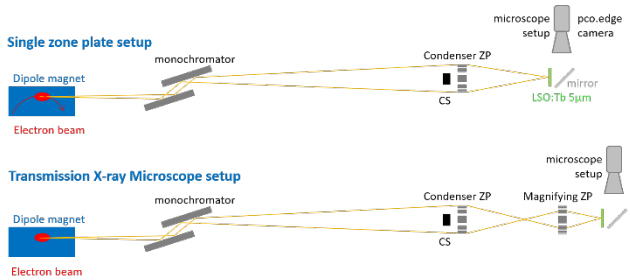

Figure 5: Sketch of the single zone plate setup (top) and the X-ray transmission microscope setup (bottom).

The vertical beam size depends on the day's machine settings and is reasonable. The horizontal beam size is a robust value. It is influenced by the beta beat. Assuming a large beta beat of 10% the variations in source size are ~3% due to this beat. The design beam in the center of the TOMCAT superbend is 55.9 µm (rms) [13].

The minimum horizontal image size could not be achieved since the horizontal and vertical foci are at different detector locations. It is suspected that the thermal bump on the first crystal of the monochromator has a lensing effect on the monochromator and the measured beam size. An excellent explanation of this effect can be found in [14].

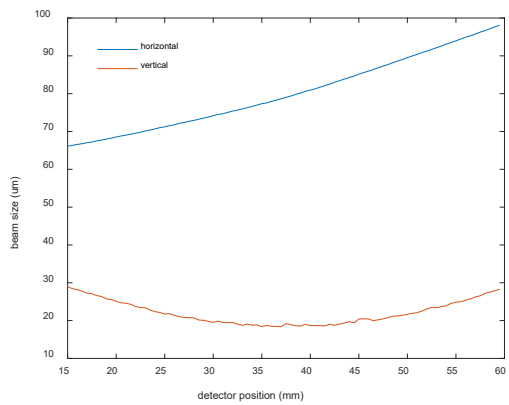

Figure 6: Vertical (red) and horizontal (blue) beam sizes, measured with single zone plate, with respect to detector position. The horizontal focus is at a different location from the vertical focus.

At TOMCAT, with the TXM setup, we achieved a total magnification of 1.01 and measured a vertical beam size of 17.3 µm (rms). In comparison to the single zone plate measurement, this is not surprising since the spot size on the scintillator due to the CZP is expected to be < 4 µm (rms), which is smaller than the scintillator thickness. At 11.5 keV, additional scintillation from the thickness will

ISBN: 978-3-95450-241-7 ISSN: 2673-5350 doi:10.18429/JACoW-IBIC2022-MOP01

blur the image. Figure 7 shows an image of the beam spot with the detector at the vertical focus of the MZP. Unfortunately, the horizontal focus location was out of the detector's range of motion.

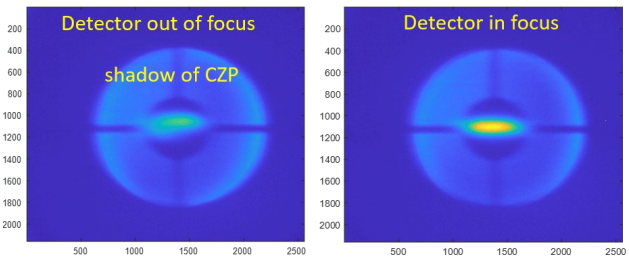

Figure 7: Image of beam focused on the detector with TXM. The vertical source size was measured as 17.3 µm rms. Horizontal minimum is out of the detector's motion range.

In the future, a larger central stop will be used so that the image of the source is completely inside the dark region of the shadow of the central stop, thus avoiding overlap with the direct X-ray beam.

CONCLUSION

For SLS 2.0, new FZP parameters will be calculated to fit the available space, photon beam wavelength, expected photon beam size at FZP location, and desired total magnification. It is also planned to use a filter before the monochromator to reduce the heat load on the monochromator crystal and consequently, the lensing effect of the thermal bump.

The new plate scintillators for the distributed loss monitors seem to be very promising. There are now 35 scintillators distributed around the storage ring for the surveillance of losses and one at the injection straight. A total of 4 loss monitor systems based on a CMOS camera readout are in operation for testing with the SLS beam. These systems will be also installed in SLS 2.0. About 100 scintillators will be distributed around the new storage ring.

ACKNOWLEDGMENTS

This work is possible with the collaboration of A. Stark, F. Barchetti, B. Zimmerli, V. Van de Vijfeijken, M. Baldinger, A. Jaggi, U. Flechsig, C. David, M. Stampanoni, K. Bitterli, R. Krempaska, G. Kotrle, E. Japichino, V. Schlott, A. Streun, M. Aiba, M. Boege, and J. Kallestrup.

REFERENCES

[1] A. Streun *et al.*, "SLS-2 Conceptual Design Report", PSI Bericht, Paul Scherrer Institut, Report no. 17-03, 2017. https://www.dora.lib4ri.ch/psi/islandora/object/psi:34977

[2] H. Braun *et. al.*, "SLS 2.0 storage ring. Technical design report", PSI Bericht, Paul Scherrer Institut, Report no. 21-02, pp. 130-134, 2021. https://www.dora.lib4ri.ch/psi/islandora/object/psi:39635

[3] C. Loch Ozkan, R. Ischebeck, and A. M. M. Stampfli, "CMOS Based Beam Loss Monitor at the SLS", in *Proc. IBIC'21*, Pohang, Rep. of Korea, May 2021, pp. 186-188. doi:10.18429/JACoW-IBIC2021-TUOB02

[4] A. Saa Hernandez, N. Milas, M. Rohrer, V. Schlott, A. Streun, Å. Andersson,, and J. Breunlin, "The new SLS beam size monitor, first results", in *Proc. IPAC13*, Shanghai, China, May 2013, paper MOPWA041, pp. 759-761.

[5] C. David, V. Schlott, and A. Jaggi, "A zone plate based beam monitor for the Swiss Light Source", in *Proc. DIPAC'01,* ESRF, Grenoble, France, 2001, paper PS13, pp. 133-135.

[6] H. Sakai *et al.*, "Improvement of Fresnel zone plate beam-profile monitor and application to ultralow emittance beam profile measurements", *Phys. Rev. ST Accel. Beams,* vol. 10, p. 042801. 2007. doi:10.1103/PhysRevSTAB.10.042801

[7] T. Scheimpflug, "Improved method and apparatus for the systematic alteration or distortion of plane pictures and images by means of lenses and mirrors for photography and for other purposes", GB Patent no. 1196, 1904.

[8] R. Ischebeck, E. Prat, V. Thominet, and C. Ozkan Loch, "Transverse profile imager for ultrabright electron beams", *Phys. Rev. ST Accel. Beams*, vol. 18, p. 082802, 2015. doi:10.1103/PhysRevSTAB.18.082802

[9] C. Ozkan Loch, D. Llorente Sancho, E. Divall, E. Ebner, P. Pollet, R. Ischebeck, and F. Loehl, "Loss monitoring for undulator protection at SwissFEL", *Phys. Rev. Accel. Beams*, vol. 23, p. 102804, 2020. doi:10.1103/PhysRevAccelBeams.23.102804

[10] EJ-204, Eljen Technology, https://eljentechnology.com/products/plastic-scintillators/ej-200-ej-204-ej-208-ej-212

[11] BCF-92, Saint Gobain – Scintillating Fibers, https://www.crystals.saint-gobain.com/radiation-detection-scintillators/fibers#

[12] K. Jefimovs, J. Vila-Comamala, M. Stampanoni, B. Kaulich, and C. David, "Beam-shaping condenser lenses for full-field transmission X-ray microscopy", *J. Synchrotron Radiat.*, vol. 15, pp. 106–108, 2008. doi:10.1107/S090904950704771

[13] Boege, M., Private Communication, 23 December 2021.

[14] M. Antimonov, A. Khounsary, A. Sandy, S. Narayanan, G. Navrotski, "On the influence of monochromator thermal deformations on X-ray focusing", *Nucl. Instrum. Methods Phys. Res., Sect. A,* vol. 820, pp. 164-171. doi:10.1016/j.nima.2016.02.103